Time-Domain Characterization of High-Speed Mid-Infrared Photodetectors Using a Laser-Based Non-Linear Vector Network Analyzer System

Mateusz Żbik[1,3]
[1]*VIGO System S.A.*
Poznańska 129/133, 05-850 Ożarów Mazowiecki, Poland
MZbik@vigo.com.pl

Jarosław Szatkowski[2,3]
[2]*National Institute of Telecomunications*
Szachowa 1, 04-894 Warsaw, Poland
J.Szatkowski@stud.elka.pw.edu.pl

Wojciech Wiatr[3]
[3]*Institute of Electronic Systems*
Warsaw University of Technology
Nowowiejska 15/19, 00-665 Warsaw, Poland
W.Wiatr@pw.edu.pl

***Abstract*—We describe a new system for broadband characterization of mid-infrared (MIR) photodetectors, manufactured by the VIGO System and encapsulated in TO-8 can. The system comprises a high repetition rate pulsed laser source, stimulating a detector in a special test fixture that is connected to ports of a vector network analyzer (VNA) with a pair of cables. After calibrating the VNA at the cable ends using the thru-reflect match (TRM) method supplemented with power and phase calibration, it operates in mode of nonlinear VNA, i.e. it is capable of measuring magnitude and phase spectra of harmonic signals both corrected for effects of systematic errors. In order to recover the differential signal at the detector reference plane on the can header, we utilize the transfer matrix of the test fixture, which counts 16 nonzero entries due to signal crosstalk in the fixture. This matrix is determined with another calibration procedure, based on measuring special built-in-house standards, mounted inside TO-8 housing. With the matrix determined, we transfer the measured spectra to the TO-8 reference plane and then convert them with IFFT to the time-domain. This approach enables recovering sub-nanosecond differential pulses of amplitudes below 1 mV and speed up performance evaluation of MIR detectors tested.**

Keywords—nonlinear vector network analyzer, infrared photodetector, QCL laser, pulse response, de-embedding.

I. Introduction

With the fast growth of the mid-infrared devices market, designers have begun to explore new applications, where the fast response time sensors are required. VIGO System manufactures infrared photodetectors with the use of mercury cadmium telluride (HgCdTe) or III-V group compounds, a unique material whose band gap may be tuned over a wide range for fast and low noise detection of 2–14 µm mid-infrared radiation. High-speed photodiodes are highly desirable in many recent applications, e.g. for transferring data of GB/s rate via MIR free-space communication links [1]. Also, they are applied in dual-comb spectroscopy systems [2] to capture multi-heterodyne down-conversion products of optical modes for mid-IR spectroscopic detection.

Despite the current era of surface mount RF devices, compact TO cans, shown in Fig. 1, are still used for packaging MIR photodetectors because of design reasons. The TO-8 detectors are equipped with miniature thermo-electric coolers (TECs) [3], that enable reducing noise and thus enhancing sensor's sensitivity, however at the cost of increased inductance of the interconnecting wires [4] limiting

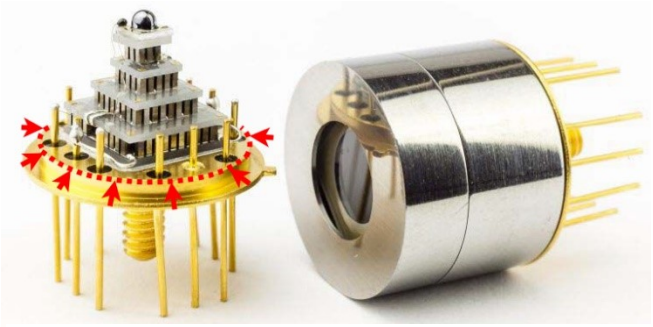

Fig. 1. LWIR photodetector in TO-8 package (right) and its inner design (left), i.e. an optically immersed sensor mounted on the top of a four-stage Peltier TEC cooler [3]. The red arrows in the left indicate the detector calibration plane.

the sensor's bandwidth and thus its speed. Similar limiting impact is also introduced by the parasitic capacitance and series resistance of the sensor's chip itself [5]. For these reasons, photodiode temporal response limitations are of high interest to the RF circuit designers. Moreover, large-signal performance characterization is equally important, since HgCdTe photodiodes are prone to saturate at moderate MIR intensities [3].

So far, high-frequency photodiode measurements in the VNA system were described by e.g. [6], [7]. The frequency-domain approach is reported to be suitable for electrical small-signal equivalent circuit modeling, however, for more advanced simulations, it is required to characterize the opto-electrical transmission coefficient of the device, as described in [8] and [9]. Moreover, analysis of the time-domain voltage and current waveforms gives essential information for modeling nonlinear behavior of the device under test, as described in [10]. Yet, those systems are designed for standard needs of optical fiber communication, as they operate in the near-infrared wavelength region (from 780 nm to 2500 nm) and thus are inadequate for testing the HgCdTe photodetectors.

Due to the lack of ready solutions for temporal measurements in the MIR range, e.g. electro-optical high-speed modulators and directly modulated lasers, we have decided to build a system by ourselves, using already developed pulsed optical signal source [11] for broadband sensor excitation. In order to measure the time-domain signal waveforms, e.g. sensor pulse response, we utilized multitone nonlinear VNA (NVNA) receivers, synchronized with harmonic phase-reference comb generators [12]-[13].

978-83-949421-6-8

Compared to the setups measuring signals in time-domain, such as mixer-based microwave transition analyzer and oscilloscope-based systems, NVNA provides much higher dynamic range (>130 dB) and doesn't suffer from time-base errors [13]-[14].

The device under test is inserted into an in-house designed and manufactured two-port fixture [15], which enables us measuring the differential- and single-ended pulse response in the frequency range up to 5 GHz. In order to provide reliable pulse response measurements, we utilized a calibration technique described in [15], extending it by the power and phase calibration as described in [13]-[14], [16].

In this paper we present a system of the NVNA combined with the pulsed laser source for opto-electric sensor characterization in the balanced setup. Thanks to high dynamics range of this system, we were able to retrieve low current (tens of μA) time-domain response of a long wavelength mid-infrared (LWMIR) photodiode without the use of any additional amplifier. Finally, we discuss potential benefits of the proposed system and de-embedding technique.

II. The Experimental Set-up

By utilizing pulse modulated infrared source we convert the NVNA into an opto-electric multi-harmonic receiving system whose schematic diagram is shown in Fig. 2. Measurement set-up details are discussed in the following subsections.

A. The mid-infrared source

For building the multi-harmonic analysis system, we utilized a quantum cascade laser based time-domain optical comb. Such unipolar devices cover emission wavelengths across the whole MIR spectrum and show capability of direct current high-speed modulation. As described in [11], fast optical pulses with time duration of less than 100 ps were measured at full width at half maximum (FWHM). To provide a pulsed light source suitable for MIR devices characterization in the NVNA system, we combined pulsed current source from [11] with a charge-line based timing circuit described in [17].

The house-made laser operates at $\lambda \approx 10$ μm and the MIR output radiation is focused to a spot of approximate diameter of φ_{FWHM}=100 μm and 100 mW peak pulse power. In order to analyze sensor response at different power levels, e.g. its large signal behavior, we applied a wire grid polarizer for adjusting the optical power.

B. TO-8 test fixture

Modulated light envelope excites the TO canned sensor, which is inserted into a special RF socket of the test fixture [15] that provides low-loss signal propagation and effective heat transfer from TEC to the ambient. The fixture, shown in Fig. 2, was developed to characterize the photodiodes in a balanced two-port configuration that maintains and exploits the symmetry of the photodetector's package pins and internal bounding wires [4]. With the fixture connected to the VNA's ports P1 and P2, we determine differential- and common-mode detector's characteristics [15].

C. NVNA system

The pulsed photocurrent signal is fed into four-port VNA (Rohde & Schwarz ZVA-50), which was converted into a complete multi-harmonic characterization system by combining two harmonic phase reference combs [16]. One of them, showed in Fig. 2, is permanently connected to the VNA's port P3 and serves as a phase reference, while the other is used only during the system calibration (see Sec IIIA). In order to maintain constant phase of the optical excitation, pulsed laser is triggered by a square wave generator, precisely synchronized by the VNA internal 10 MHz reference clock.

Auxiliary equipment such as temperature controller (VIGO System PTCC) and precision DC power supply shown in Fig. 2 was used for HgCdTe photodetector cooling and setting its bias for optimal high-speed conditions [5].

III. Calibration

In order to accurately measure DUT's pulse response in the time- and frequency-domains, the system requires the use of specific calibration techniques [13]-[16]. At first, the

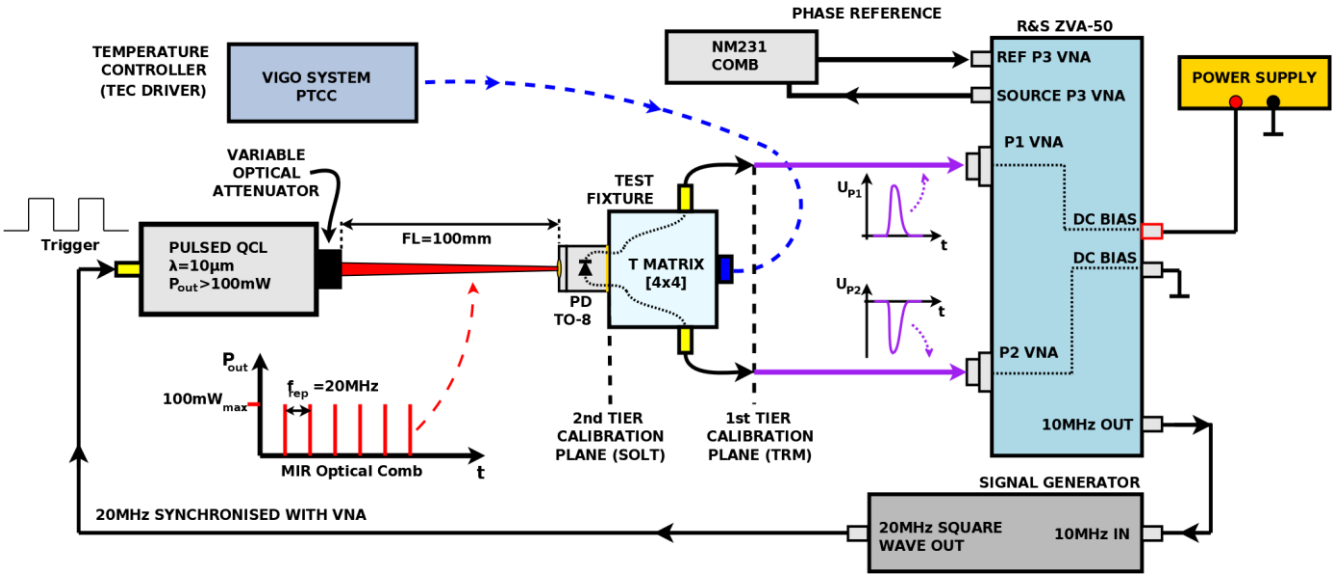

Fig. 2. Schematic diagram of the NVNA system for characterization of photodiodes mounted in TO-8 can.

relative wave measurements are performed at each harmonic of the measured spectrum to establish the measurement reference planes at the TO-8 housing base, marked in Fig. 1 with red arrows. However, to capture high-speed pulsed signals, this typical S-parameter procedure needs to be extended by an absolute power calibration with a power sensor. Finally, we connect a pair of harmonic phase reference (HPR) generators to calibrate NVNA for phase [13, 16].

A. S-parameter calibration

We employ a two-tier calibration procedure which at first is performed with a standard thru-reflect-match (TRM) calibration, carried out with the use of SMA connectorized standards. It establishes the reference plane at the SMA fixture connectors -- see in Fig. 2.

The fixture embedding a two-port device, is typically represented as a linear four-port network, showed in Fig. 3. Its transmission matrix counts 16 nonzero entries, due to noticeable cross-talk between the fixture ports. This matrix is determined with a set of four short-open-load-thru (SOLT) standards [15]. The standards were built in house on TO-8 header reference plane, marked in Fig. 1 with red arrows.

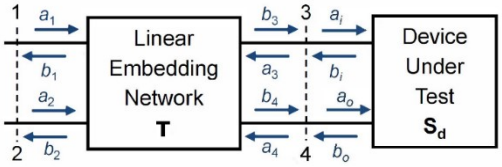

Fig. 3. A four-port model of the fixture with a two-port device [15].

For de-embedding the fixture, we apply the T-matrix in a block form [15]:

$$\begin{bmatrix}\mathbf{b_m}\\ \mathbf{a_m}\end{bmatrix} = \begin{bmatrix}\mathbf{T_{11}} & \mathbf{T_{12}}\\ \mathbf{T_{21}} & \mathbf{T_{22}}\end{bmatrix}\begin{bmatrix}\mathbf{a}\\ \mathbf{b}\end{bmatrix}, \quad (1)$$

where square block matrices $\mathbf{T_{11}}$, $\mathbf{T_{21}}$, $\mathbf{T_{12}}$ and $\mathbf{T_{22}}$ are of size 2x2, the vectors of waves:

$$\mathbf{b_m} = [b_1 \quad b_2]^T, \qquad \mathbf{a_m} = [a_1 \quad a_2]^T,$$
$$\mathbf{a} = [a_3 \quad a_4]^T, \qquad \mathbf{b} = [b_3 \quad b_4]^T,$$

represent measured and original signals at relevant ports, respectively.

In order to retrieve the original signals, we invert the transformation (1) getting:

$$\begin{bmatrix}\boldsymbol{a}\\ \mathbf{b}\end{bmatrix} = \begin{bmatrix}\mathbf{T_{11}} & \mathbf{T_{12}}\\ \mathbf{T_{21}} & \mathbf{T_{22}}\end{bmatrix}^{-1}\begin{bmatrix}\boldsymbol{b_m}\\ \boldsymbol{a_m}\end{bmatrix}, \quad (2)$$

from which it is easy to calculate incident and reflected waves at the 2nd tier TO-8 calibration plane (ports 3 and 4 shown in Fig. 3).

B. Power and phase calibration

Since a nonlinear characterization requires the knowledge of waves instead of wave ratios, the S-parameter of the first tier calibration needs to be extended. To this end we connected a calibrated microwave power meter to port P1 of the NVNA for measuring the power generated by the NVNA and determining the absolute amplitude of the measured time-domain waveforms.

In order to characterize the phase relationships between the harmonics present in the measured spectra [13], we utilized a pair of HPR generators. One of the HPRs shown in Fig. 2 is permanently connected to the P3 of the NVNA and serves as a phase reference for all measurements. Then, we connect the other HPR to SMA connectorized cables in order to determine the phase relations at a calibration planes set during the previous TRM procedure. This calibration step is based on a known phase of two HPR generators, since the phase relationships between the frequency components of those multi-harmonic generators is defined by the manufacturer. Consequently, by measuring the sensor's pulse response and comparing it with reference signal at NVNA's P3, we are able to correct the measured signals of a DUT for phase.

IV. Measurements

To verify our approach and apply calibration procedures, we employed the NVNA opto-electrical system for measuring response of the HgCdTe LWMIR photodiode (VIGO System PVI-4TE-10.6-1x1) at temperature T=205 K and recommended bias voltage of V_b=-0,7 V [5]. We defined the measurement frequency grid from 20 MHz up to 5 GHz (250 harmonics) in order to exploit optimal performance range of the TO-8 fixture [15].

To avoid saturation effect of photodiode due to its large signal operation, the optical comb peak power should not exceed 100 µW [3]. This power level corresponds to approximately 10 mV of pulsed electrical signal at 50 Ω load, therefore to provide receiver high dynamic range, the VNA's resolution bandwidth was narrowed down to 10 Hz and the internal attenuators at the receiver inputs were set at 0 dB.

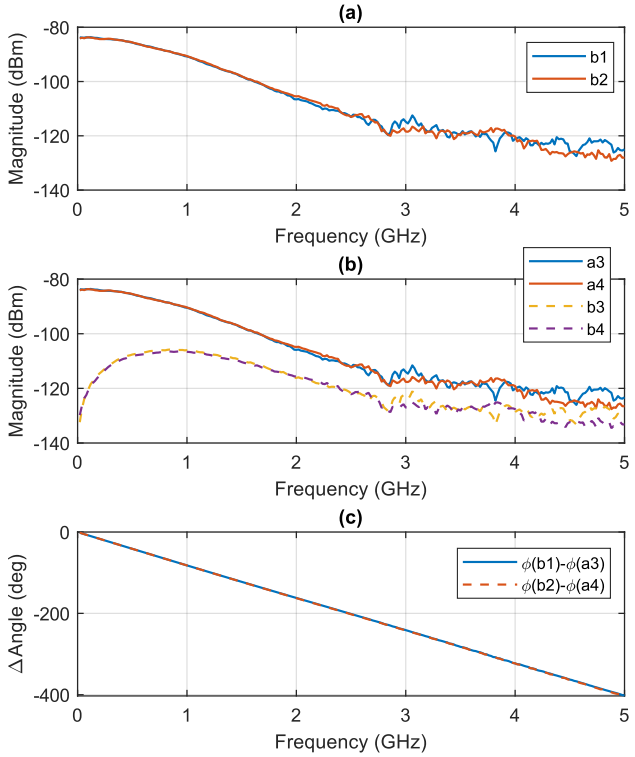

Fig. 4. Incident waves in the SMA calibration plane (a), incident and reflected waves in the TO-8 calibration plane (b) and phase difference between VNA received (b_1, b_2) and incident waves a_3 and a_4 (c).

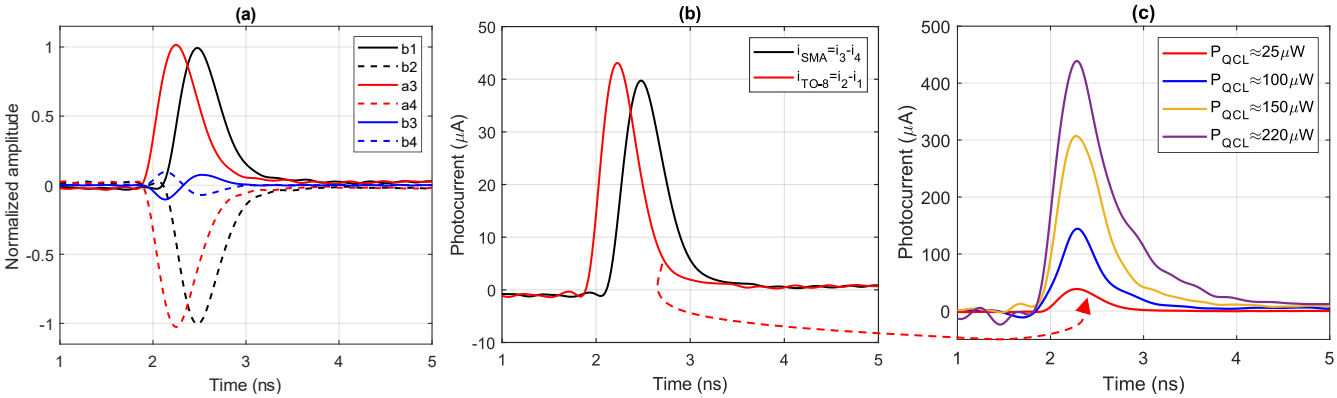

Fig. 5. Measured photodiode pulse responses at relevant reference planes: normalized single-ended signal pairs (a), pulsed photocurrent waveforms (b) and photocurrent waveforms at higher light intensities (c).

With the laser radiation aligned on the sensor's active area, we captured frequency-domain signals at the SMA fixture's ports as shown in Fig 4(a). Then we applied the de-embedding formula (2) on the received waves b_1 and b_2, recovering incident and reflected waves at the TO-8 calibration plane shown in Fig. 4(b). The magnitudes of incident waves a_3 and a_4 (see Fig. 3) tend to decline more than 5 dB at 1 GHz mainly due to the sensor's parasitic series inductance and parallel capacitance of approximately 18 nH and 10 pF respectively [4], [6]. As one can notice, the magnitudes of reflected wave's b_3 and b_4 initially increase and then peak at approximately 800 MHz due to growing port mismatch of the fixture [15]. Nonetheless, harmonics of interest are properly captured down to -110 dBm due to the system dynamic range limited by the VNA noise floor for frequencies exceeding 2.7 GHz.

Phase spectrum of the de-embedded signals a_3, a_4, determined in relation to the NVNA received signals b_1 and b_2, is presented in Fig. 4(c). The recent shows noticeable phase shift of received harmonics due to applied de-embedding formula (2).

To retrieve the pulse response of the sensor, we transformed the frequency-domain signals showed in Fig. 4 to temporal waveforms with an inverse fast Fourier transform (IFFT) algorithm. As a result, we obtained single-ended signal pairs (b_1,b_2), (a_3,a_4) and (b_3,b_4) of normalized amplitude to show time-domain relationships - see Fig. 5(a). Due to the differential signaling design of fixture waveforms within each pair are counter-phase. Making use of the absolute power calibration, we converted relative measurements from Fig. 5(a) to a flow of the photocurrent generated in the excited sensor's junction, as shown in Fig. 5(b). In Fig. 5(c) we excited the sensor with higher power light pulses to capture and characterize its large-signal performance.

As one can notice in Fig. 5(b), the de-embedded pulse response at TO-8 header (red line) precedes the measured one (black line) and features a higher amplitude due to the removed impact of the test-fixture, i.e. time delay and losses. According to the frequency-domain phase difference shown in Fig. 4(c), this time delay is about 220 ps. The rise time and fall time of an original pulse in Fig. 5(b) ($t_{r\,TO\text{-}8}$=200 ps, $t_{f\,TO\text{-}8}$=460 ps) are shorter, than measured at fixture SMA ports ($t_{r\,SMA}$=220 ps, $t_{f\,SMA}$=520 ps). Therefore the actual photodiode response characteristics can be determined solely through the de-embedding process.

Fig. 5(c) portrays response of the photodiode to increasing MIR power stimulation. As it is evident, the amplitude of the temporal signals increases too, however their shape deteriorates at higher levels. This effect is caused by excess number of generated carriers in the semiconductor junction and is called saturation. The saturation results in higher capacitance and lower dynamic resistance of the sensor's junction [3], which combined with parasitic series resistance and inductance (approx. 10 Ω and 18 nH, respectively) extends the time necessary to remove the excess charge from the semiconductor [5].

The unique feature of multi-harmonic VNA measurement enable us to determine the upper signal level for linear operation of the detector, i.e. define the maximum power for its optimal high-speed performance. For this particular sensor, the MIR optical power shouldn't exceed 50 µW if the pulse response fall time $t_{f\,TO\text{-}8}$ is to be shorter than 480 ps.

V. Conclusions

We presented a novel approach to MIR photodiodes pulse response characterization with the use of a multi-harmonic VNA. Since this system requires a broadband MIR signal source, we employed a pulsed quantum cascade laser source for LWMIR photodiode excitation. We applied a SOLT calibration [15] method to first characterize the test fixture with its 4x4 transmission matrix, and then used a power sensor and a pair of comb generators to establish absolute power and phase reference for signal measurements.

Finally, we experimentally confirmed the usability of the electro-optical NVNA setup for time-domain characterization of TO-8 canned devices at subnanosecond and large-signal operation. The total system root mean square (RMS) noise level lower than 0.3 μA_{RMS} enabled us to perform broadband photocurrent measurements without the use of additional amplifiers.

This new solution can be easily adapted to characterize a broadband circuits mounted in other types of TO packages. Moreover, by using different wavelength laser sources our system might be adapted to characterization of various types of devices e.g. fiber-optic communication receivers operating in the frequency range of up to 40 GHz as suggested in [16].

REFERENCES

[1] J. Mikołajczyk, “An overview of free space optics with quantum cascade lasers,” Int. J. Electron. Telecom., vol. 60, no.3, pp. 259-263, 2014.

[2] G. Villares, F. Cappelli, A. Hugi, et al., "Dual-comb spectroscopy based on quantum cascade laser frequency combs," 2015 Conf. Lasers and Electro-Optics (CLEO), San Jose, CA, 2015, pp. 1-2.

[3] J. Piotrowski. and A. Piotrowski, "Room temperature photodetectors," Mercury Cadmium Telluride: Growth, Properties and Applications, P. Capper and J. Garland, Ed. NewYork,Willey, 2010, pp.513-537.

[4] W. Wiatr, L. Opalski, J. Piotrowski and M. Krysicki, "Modeling interconnects for thermoelectrically cooled infrared detectors," 2016 21st Int. Conf. Microw., Radar and Wireless Commun. (MIKON), Krakow, 2016, pp. 1-4.

[5] J. Pawluczyk, J. Piotrowski, W. Pusz, et al., “Complex behavior of time response of HgCdTe HOT photodetectors,” Jour. Elec. Mater., 44:3163, Jun. 2015.

[6] K. Opalska, L. J. Opalski, W. Wiatr, et al., "Small-signal lumped-element equivalent model for high operating temperature infrared photodetectors," 2016 21st Int. Conf. Microw., Radar and Wireless Commun. (MIKON), Krakow, 2016, pp. 1-4.

[7] D. Fink, R. Mirzoyan, M. Teshima and O. Reimann, "Measurement and modeling of silicon photomultiplier devices by means of S-parameter techniques," 2014 IEEE Nucl. Sci. Symp. and Med. Imag. Conf. (NSS/MIC), Seattle, WA, 2014, pp. 1-4.

[8] B. Elamaran, R. D. Pollard and S. Iezekiel, "Implementation and calibration of a two-port electrooptic network analyzer," IEEE Microw. and Guided Wave Lett., vol. 9, no. 9, pp. 369-371, Sept. 1999.

[9] A. Ferrero, G. Ghione and M. Pirola, "A new, simple, test-set for on-wafer characterization of millimeter-wave electro-optic devices," 2000 IEEE MTT-S Int. Microw. Symp. Digest, Boston, MA, USA, 2000, pp. 1607-1610 vol.3.

[10] A. Ghose, B. Bunz, J. Weide and G. Kompa, "Extraction of nonlinear parameters of dispersive avalanche photodiode using pulsed RF measurement and quasi-DC optical excitation," IEEE Trans. Microw. Theory Techniques, vol. 53, no. 6, pp. 2082-2087, Jun. 2005.

[11] M. Żbik, "Sub-nanosecond pulsed quantum cascade laser driver," 2019 Conf. Lasers and Electro-Optics (CLEO), San Jose, CA, USA, 2019, pp. 1-2.

[12] M. Vanden Bossche, "Switching amplifier design with S-functions, using a ZVA-24 network analyzer," ESA Microw. Technol. and Techniques Workshop, 2010

[13] J. Verspecht, "Large-signal network analysis," IEEE Microw. Mag., vol. 6, no. 4, pp. 82-92, Dec. 2005.

[14] D. Barataud, C. Arnaud, B. Thibaud, et al., "Measurements of time-domain voltage/current waveforms at RF and microwave frequencies based on the use of a vector network analyzer for the characterization of nonlinear devices-application to high-efficiency power amplifiers and frequency-multipliers optimization," IEEE Trans. Instrum. Meas., vol. 47, no. 5, pp. 1259-1264, Oct. 1998.

[15] W. Wiatr, B. Łączyński, J. Piotrowski, et al., "A broadband test fixture for characterizing circuits mounted inside TO-8 package," 2015 IEEE Int. Conf. Microw., Commun., Antennas and Electron. Syst. (COMCAS), Tel Aviv, 2015, pp. 1-4.

[16] NMDG, *Extension kit for R&S Vector Network Analysers Characterisation of Nonlinear RF/HF Components in Time and Frequency domain*. (2011). [Online]. Available: http://www.nmdg.be/

[17] M. Żbik and P. Wieczorek, “Charge-line dual-FET high-repetition-rate pulsed laser driver,” Appl. Sci., vol. 9, no. 7, p. 1289, Mar. 2019.